Mon. Not. R. Astron. Soc. **000**, 1–7 (2014) Printed 26 September 2021 (MN LATEX style file v2.2)

Ultra-luminous X-Ray sources with wind Roche lobe overflow in Ring galaxies

Hao-Tian Song[1] and Zhao-Yu Zuo[1,2⋆]
[1] *Department of Physics, School of Science, Xi'an Jiaotong University, Xi'an 710049, China*
[2] *Key laboratory of Modern Astronomy and Astrophysics (Nanjing University), Ministry of Education, Nanjing 210093, China*

26 September 2021

ABSTRACT
Ultra-luminous X-ray sources (ULX) are binaries containing a nondegenerate companion and a black hole (BH) or neutron star (NS), drawing great attention due to their super-Eddington luminosity. We have presented the comprehensive evolution model for ULXs in Ring galaxies including wind Roche-Lobe overflow mechanism. The wind-fed ULXs contributes more to population than traditional Bondi-Hoyle-Lyttleton (BHL) mode. Seven galaxies was adopted as example of star burst galaxies and X-ray luminosity function (XLF) was compared between observation and simulation. We predicted that donor mass is $2.7M_{\odot}$ and orbit period is few days in typical ULXs. Most of donor star are H donor stars, indicating active evolution stage.

Key words: methods: statistical — galaxies: star-burst — stars: evolution — X-ray: binaries — stars: distribution

1 INTRODUCTION

As off-center, point-like sources with isotropic equivalent X-ray luminosity $L_X > 10^{39} erg \cdot s^{-1}$, ultra-luminous X-ray sources (ULXs) have been focused on by plenty of observational and theoretical work (see Kaaret et al. 2017, for reviews). Generally ULXs are regarded as tail of high mass X-ray binaries (HMXB). The mechanism of ULXs is accretion of X-ray binaries. The compact stars are thought to be Black Holes (BH) before discovery of pulsing ultra-luminous X-ray source (PULXs) in M82 X-2 (Bachetti et al. 2014) with $L \simeq 1.8 \times 10^{40}\mathrm{ergs}^{-1}$. Neutron Stars (NS) mostly accompany by pulsar-like dipole field strengths $10^{11} \lesssim B \lesssim 10^{13}\mathrm{G}$ which allows several descriptions of the observed properties (King et al. 2017; Middleton et al. 2019).

As the luminosity of $10^{39} erg \cdot s^{-1}$ is the Eddington luminosity of a $10M_{\odot}$ BH, the majority of ULXs is super-Eddington isotropic accretion. However, assumption of geometrical beaming (King et al. 2001) can avoid breaching the Eddington luminosity with support of accretion disk simulation (Jiang et al. 2014; Ohsuga & Mineshige 2011). King (2009) gave an example of collimated radiation with $L > 3L_{Eddington}$. Furthermore, beaming factor in NS are correspondingly lower than BH with the same Mass transfer (MT) rate, which indicates that PULXs dominate the region of higher luminosity (King & Lasota 2016).

Previous theoretical simulation mostly indicates the stable RL overflow is the primary method for ULXs (Shao & Li 2015; Wiktorowicz et al. 2019a; Shao et al. 2019), which all implied the BHL mass transfer mode for wind overflow. For instances, Shao & Li (2015) utilized evolutionary population synthesis to reconstruct the evolution of NS ULXs. The simulation generally displays the mass-orbital plane and the predicted amount of NS ULXs in M82 and MW-like Galaxies. More specific systematic study in MW galaxies for NS ULXs indicates that donor star tends to be helium star (Shao et al. 2019). Furthermore, specific simulation via StarTrack EPS code was conducted by Wiktorowicz et al. (2019a), who took geometrical beaming into account. Assuming individual metallicity, They drew the conclusion that BH emits radiation isotropically while NS predominantly, and BH ULXs outnumber NS ULXs which is inconsistent with observation. Recently, wind-powered simulation by Baker et al. (2013) demonstrates that the majority of specific ULXs (red super-giant companion) transfer mass via wind-fed mode. However, the formalism of WRL developed by (Abate et al. 2013) was just adoptable for narrow region of parameters, whereas donors stars need to be carbon-enhanced metal-poor stars. As consequence, the observation is hard to be related to simulation results in such a strict condition. Another research about wind Roche-lobe overflow cases Zuo, Zhao-Yu et al. (2021) emphasized the enhancement of wind accretion mechanism and displayed the predicted binary parameters of NS ULXs.

Ring Galaxies are ideal laboratories for binaries evolution research. Although they contribute to a small distri-

⋆ E-mail:zuozyu@xjtu.edu.cn

bution (Wolter et al. 2018a, approximately $0.02\% - 0.2\%$ of all spiral galaxies), particular and energetic environment without contamination from spurious sources is suitable for studying binary evolution. The reason of burst star forming in Ring Galaxies is encounter with nearby galaxies, which implies that the age of stars is similar. Besides, most ULXs formulation environment is normal sharing similar metallicity (Wolter et al. 2018). Additionally, with high star forming rates (SFR) and shorter evolution duration, Ring Galaxies share more similarity with assuming environment, which avoids the various initial conditions of EPS. According to (Wolter et al. 2015), remarkable number of ULXs was detected in Star-burst galaxies strongly supports our simulation.

In this work, we utilize the advanced WRL mechanism for the BPS of ULXs, and predicted ULXs' number and population in Ring galaxies. The evolution parameters are comply the characteristics of Ring galaxies and observation X-ray luminosity function is used to be compared with simulation.

2 METHODS

We utilized the Evolutionary population synthesis (EPS) code initially developed by Hurley et al. (2002) with further updates, which are briefly described as follows. And MESA program was performed in the population synthesis of NS for more specific evolution.

The Initial Mass Function (IMF) developed by Kroupa et al. (1993) was applied. Although the shapes of IMF differ significantly, it is less subject to the uncertainty due to the similarity of the IMFs for larger masses. The mass of star on zero-age sequence (ZAMS) satisfies the following distribution with initial mass ranging from 2 $M_\odot$ to 150 $M_\odot$.

$$\xi(m) \propto m^{-\alpha} \tag{1}$$

where

$$\alpha(m) = \begin{cases} +0.3 \pm 0.7 & 0.01 \leqslant m < 0.08 \\ +1.3 \pm 0.5 & 0.08 \leqslant m < 0.50 \\ +2.3 \pm 0.3 & 0.50 \leqslant m < 1.00 \\ +2.3 \pm 0.7 & 1.00 \leqslant m \end{cases} \tag{2}$$

The distribution of mass ratios q ($q = M_1/M_2$) was uniform between 0.08 and 1 by steps of 0.10 (Wiktorowicz et al. 2019b). The orbital separation was ranged from 3.0 to $10^4 R_\odot$ which facilitates the comparison with other models (Yungelson et al. 1997). Here we assumed that $ln(a)$ is uniformly distributed. According to the previous analysis Wolter et al. (2018), produced stars are younger than 300Myr and majority of them is consistent with age of HMXBs. Therefore, the maximum evolution time was set to 200Myr in isolation. As for supernova kicks, we draw them from a Maxwellian distribution with $\sigma = 265km \cdot s^{-1}$ (Hobbs et al. 2005). And subsolar metallicity $Z = 0.5Z_\odot$ was adopted in our simulations which is the metallicity prediction of environment (Wolter et al. 2018). Furthermore, metallicity is a key factor affecting the evolution (Zuo, Zhao-Yu et al. 2021).

For sources undergoing Roche Lobe Overflow (RLOF) mass-transfer, the traditional formula was used for sub-Eddington accretion rates, where Eddington luminosity is approximately $L_E = 1.6 \times 10^{38} m_1$ for hydrogen-rich material. Supplied with super-Eddington mass transfer rates, the accretor expel matter in significantly different approach. Outside the spherization R_{sph} (Blundell et al. 2007), accretion luminosity is released as usual (Shakura & Sunyaev 1973; Poutanen et al. 2007). But within R_{sph}, radiation become inefficient and the outflow maintain energy release in L_E under the pressure of radiation. Bolometric luminosity L_X is

$$L_X = \begin{cases} L_{\rm Edd}\,(1 + \ln \dot{m}_{\rm tr}) & \dot{m}_{\rm tr} > 1 \\ L_{\rm Edd} \dot{m}_{\rm tr} & \dot{m}_{\rm tr} \leqslant 1 \end{cases} \tag{3}$$

Where $\dot{m}_{\rm tr} = \dot{M}_{\rm tr}/\dot{M}_{\rm Edd}$ and $\dot{M}_{\rm tr}$ is in units of $M_\odot/yr$. For the region within R_{sph}, a biconical geometry is formed with collimation of radiation (King 2008). Therefore, the finite cones can be detected by observer. The apparent (isotropic) X-ray luminosity is

$$L_{app} = L_X/b \tag{4}$$

Where b is beaming factor defined as the fraction of funnels area, $b \overset{\rm def}{=} \Omega/4\pi$, and Ω is the combined solid angle of both beams. When $\dot{m}$ is larger enough, the scales can vary from the typical cylinderical radius to R_{sph} markedly. And for soft-excess luminosity, the observed relation $L_{\rm soft} \propto T^{-4}$ sustain the estimated value of b (King 2009).

$$b = \begin{cases} 1 & \dot{m}_{\rm tr} \leqslant 8.5 \\ \frac{73}{\dot{m}_{\rm tr}^2} & 8.5 < \dot{m}_{\rm tr} \end{cases} \tag{5}$$

whereas for $\dot{m} < 8.5$, it is assumed unbeamed. And this formula have been verified in plenty of hyperluminous X-ray sources (King & Lasota 2014, 2016; King et al. 2017). In addition, there was an implication (Wiktorowicz et al. 2017) that extremely beamed sources are scarce and transient that lead to difficulty in detection. That means there is no lower valve for the beaming factor. For CE evolution during this process, the energy budget approach have been implied (Webbink 1984, 2008) and we set $\alpha_{CE} = 0.9$ suggested by Zuo & Li (2014).

Furthermore, the wind Roche lobe overflow (WRL) could be taken into account. The traditional Bondi-Hoyle-Lyttleton (BHL) MT formula for WRL (Bondi & Hoyle 1944; Edgar 2004) is

$$\dot{M}_{\rm BHL} = \pi R_{\rm BHL}^2 v_{\rm rel} \rho \tag{6}$$

where $\dot{M}_{\rm BHL}$ is the mass accretion rate, $v_{\rm rel} = \sqrt{v_\beta^2 + (v_{\rm orb}[q/(1+q)])^2}$ is relative speed between the wind and compact object. $v_{\rm orb}$ is orbital speed given by $v_{orb} = 2\pi a/P_{orb}$ with P_{orb} being the orbit period. $R_{BHL} = 2GM_\bullet/v_{\rm rel}^2$ is the modified accretion radius and ρ is the density of the wind at orbital separation. After assumption of isotropic dilution of the wind, the fraction of wind captured $\mu_{\rm BHL} = \dot{M}_{\rm BHL}/\dot{M}_\star$ can be:

$$\mu_{\rm BHL} = \frac{(1+q)/q^3}{\eta(1-f\mathcal{E})^\beta \left[1 + (\eta(1+q)(1-f\mathcal{E})^\beta/q)\right]^{3/2}} \tag{7}$$

where $\mathcal{E}$ is the ratio of stellar Roche lobe radius by the orbital separation and only related to q (Eggleton 1983), and η is the speed ratio. We adopt this model for fast wind accretion. However, another research (El Mellah et al. 2019) proposed that ULXs could remain stable in WRL with a

Table 1. Properties of Ring galaxies applied in this work.

Name	Distance (Mpc)	SFR ($M_\odot/yr$)	Z ($Z_\odot$)
Cartwheel	122	20	0.14
NGC 922	48	8.0	0.5-1.
Arp 147	133	4.1	0.19-0.40
AM 0644-741	91.6	2.6	0.45
Arp 143	57.1	2.3	0.44-0.71
Arp 148	145.2	2.5	
Arp 284	37	4.0	0.19-0.38

highly beamed wind. Based on realistic acceleration profiles, they estimated the MT by computing the bulk motion of the wind. By assuming non-isotropic dilution of stellar wind, the fraction of wind captured can be significantly higher especially for higher wind speed ratio. And several binary systems have been proved possible for WRL, such as M101 (Liu et al. 2013), and P13 (Fürst et al. 2018). We adopted his simulation and assume μ as a function of η, stellar filling factor, β and mass ratio q. The WRL efficiency systematically improved. And WRL can be a possible mechanism for ULXs. In this mechanism, the value of the wind velocity is not accurate during the simulation. As suggested by Belczynski et al. (2008), it was proportional to the escape velocity from the surface of the mass-lossing star

$$V_{\rm wind}^2 = 2\beta_{\rm wind}\frac{GM_{\rm don}}{R_{\rm don}} \tag{8}$$

where $M_{\rm don}$ and $R_{\rm don}$ are the mass and radius of donor star respectively. $\beta_{\rm wind}$ depends on the spectral type of the donor star. For main Sequence stars, we adopted a linear interpolation from $\beta_{\rm wind} = 0.5$ for lower massive stars ($< 1.4M_\odot$) to $\beta_{\rm wind} = 7$ most massive stars ($> 120M_\odot$) Lamers et al. (1995). The $\beta_{\rm wind}$ of extended H-rich stars ($R_{\rm don} > 900R_\odot$) was set to 0.125 due to slow winds. As for He-rich stars, $\beta_{\rm wind} = 7$ when $M_{donor} > 120M_\odot$ (the same as MS stars) and $\beta_{\rm wind} = 1.3$ when $M_{donor} < 10M_\odot$, and we interpolated in between.

As for the observation of ULXs, the statistics of ULXs in seven galaxies have been published (Wolter et al. 2018a). Relevant properties are listed in Tab. 1. All the metallicity of these galaxies are sub-solar and similar to each other. For numerical comparison with them, the evolved population of binaries should be in conjunction with a realistic birth rates and metallicity. Here the distribution of each binary system is

$$\delta r_j = \overline{S_b}\Phi\left(\ln M_{1j}\right)\varphi\left(\ln M_{2j}\right)\Psi\left(\ln a_j\right)\delta\ln M_1\delta\ln M_2\delta\ln a \tag{9}$$

where r is the rate of particular population, and $\overline{S_b}$ is the binary star forming rate (SFR) in units of $number/year$ which can be obtained from following formula with SFR in units of $M_\odot/yr$ for binaries massive than 5 $M_\odot$ (Grimm et al. 2003):

$$\overline{S_b} = (\frac{M_{low}}{5})^{1-\alpha}\frac{(\alpha-2)SFR}{5(\overline{3}+\overline{q})(\alpha-1)} \tag{10}$$

where M_{low} is the lower limit initial mass for EPS. For summation of seven galaxies $SFR \approx 42M_\odot/yr$, $\overline{S_b} = 1.5039yr^{-1}$ The total number N should be the summation of every binary system distribution. However, the number observed could differ in consideration of beaming effect. With assumption of linear relation between the area of the flux sphere and beaming factor, the chance probability is therefore $P \propto b$ (Middleton & King 2017). The observed number N_{OBS} is

$$N_{OBS} = \sum\delta N = b\sum\delta r\delta T \tag{11}$$

where δT is the duration of particular binary evolution stage. For mesa simulation, δr was obtained from EPS code where particular event is the birth of NS.

3 SIMULATION RESULTS

The simulation in this section was performed with constant SFR and metallicity. Maximal evolution time is 200Myr for early formed Ring galaxies. Because SFR in Star-burst galaxies are relatively high ($SFR > 4.5M_\odot yr^{-1}$), it is reasonable to assume that the number of ULXs is linear to constant SFR in this algorithm which accords with previous work (Mineo et al. 2013). With assumption of constant SFR for observed galaxies, we compare it with observation and previous analysis. Taking complex episodes of star forming into account, estimates should be modified via a more realistic method. We adopt EPS code developed by Hurley et al. (2002) for the evolution of BH binaries while NS binaries we implied the MESA for detailed simulation of several episodes.

Ring galaxies are comparatively rare (15 out of 345 galaxies), in which, however, the ULXs occupy the certain proportion. According to Wang et al. (2016), the observation analysis feature of star-burst galaxies (i.e., the shape of XLF and) is distinct with others galaxies which deserves our attention. Ring galaxies can imply general characteristics of ULXs due to its pure environment and burst star forming. Furthermore, young galaxies provide pure environment for star evolution and prediction of early-type galaxies share more similarity with population synthesis (see Figure 15 in Kovlakas et al. 2020). We have conducted our calculation to compare them with galaxy-focused observations (Wolter et al. 2018a). The result of X-ray luminosity function (XLF) is presented in Fig. 1.

The estimated numbers of ULXs are based on Eq. 9. The summation of the SFR for 7 galaxies is approximately $43.5M_\odot$ obtained from $L_{H\alpha}$ (Appleton & Marston 1997). Uncertainty of measuring SFR should be noticed which leads to the uncertainty of our simulation result. Therefore the observation of other limited galaxies may not be representive and comparable to our simulation. 50 sources above the ULXs valve ($10^{39}erg\cdot s^{-1}$ suggested by Kaaret et al. (2017)) are collected of which 23 sources are above $5\times10^{39}erg\cdot s^{-1}$. The simulation XLF generally fits the observation and display the characteristics of ULXs. Statistical research (Swartz et al. 2011) have been done including 107 identified ULXs in 127 nearby galaxies and differential function of XLF shows a power-law slope. The statistical simulation has been compared with observation Wolter et al. (see Fig. 5 in 2018b). The difference between star-burst galaxies and nearby galaxies is obvious in XLF, where the XLF in nearby galaxies show steeper decrease. Besides, XLF in HMXBs (Grimm et al. 2003) is also impossible to fit this in star-burst galaxies. Because the census of these galaxies is not suitable for our simulation for starburst galaxies due to their unique evo-

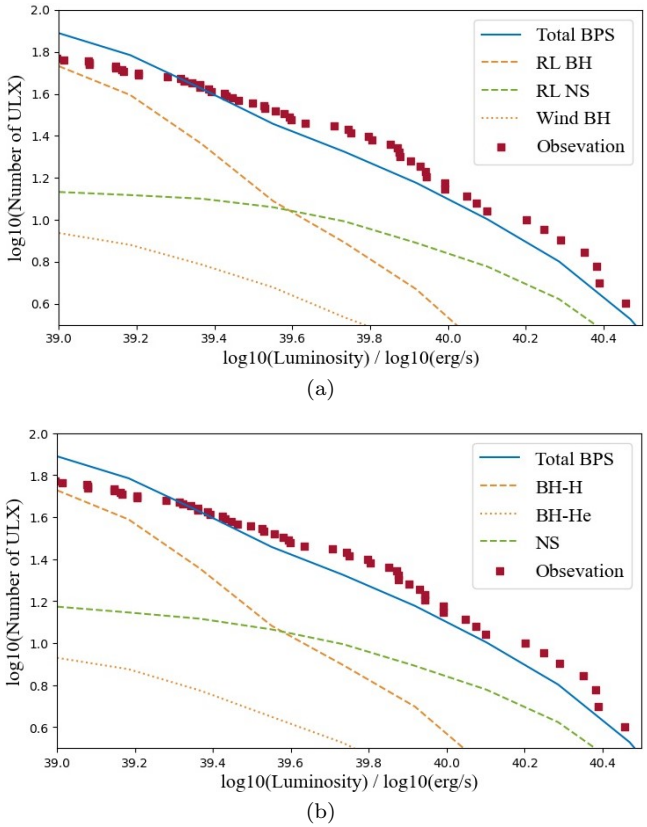

Figure 1. X-ray luminosity function (XLF) for seven Ring galaxies mentioned above. The solid blue line represents total ULXs number via EPS simulation, and red dots represent observation. (a) Dashed dotted lines represent the ULXs number in Roche Lobe accretion and wind accretion respectively. The compact star is BH and NS for pale blue and green lines respectively. (b) The simulation distribution of ULX donor and compact star. Dashed and dotted lines are ULX with Hydrogen rich and Helium rich donor star respectively, and orange lines are BH compact star while green line is NS.

lution stage and environment. However, these are requisite for EPS research.

According to the EPS simulation result, there is a break at approximately $3\times10^{40}erg\cdot s^{-1}$ which accords with the observation of other galaxies (Mineo et al. 2012; Swartz et al. 2011). The XLF break correspond to the Eddington luminosity of NS (Belczynski & Ziolkowski 2009). Although extreme objects reaching a peak luminosity of $10^{41}erg\cdot s^{-1}$ exist Gao et al. (e.g., 2003, M82), they are candidates for Intermediate Mass Black Holes (IMBHs) with masses in between $(10^2-10^5M_\odot)$ (Kuranov et al. 2007; Greene et al. 2020). With completely disparate formation scenarios, IMBHs exclude from consideration in this work. Although there is small probability of forming extremely luminous sources ($L_X > 3\times10^{40}erg\cdot s^{-1}$) in our simulation, they demand high beaming factor and correspondingly are impossible to be detected. Additionally, the observation in Ring galaxies of those cases is also limited, so we focus on middle part of XLF.

The accretion via WRL contributes quiet a few by implying this nonisotropic mechanism. Although accretion fraction μ is smaller than 20% in WRL and must be less

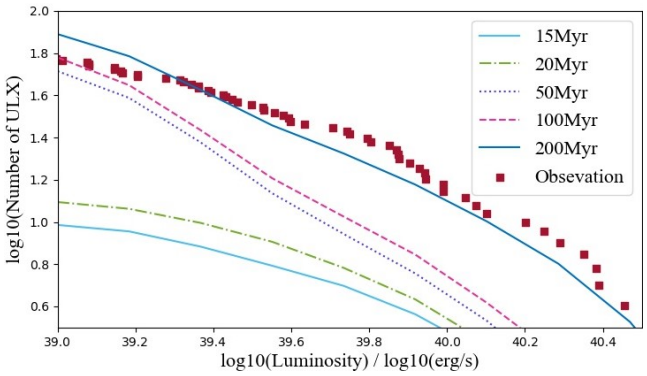

Figure 2. XLF for various evolution duration of ULXs for 200 Myr, 100 Myr, 50 Myr, 20 Myr, 15 Myr.

than 50% (Mohamed & Podsiadlowski 2011) which means most mass is lost during the accretion, ULXs via WRL exist and can reach luminosity at $5\times10^{40}erg\cdot s^{-1}$. In our simulation, high donor star mass and considerable mass transfer rate provide enough fuel for X-ray radiation. For WRL, Roche Lobe is brimming with donor star where situation is unstable in RL overflow. Consequently, mass ratio limit for donor star is more strict in RL overflow than WRL. In our simulation, high mass ratios of WRL (larger than 3) and heavy donor masses ($>10M_\odot$) are common in WRL cases, while it's unstable for RLOF. We can conclude that accretion could be stable in these evolution stage via WRL which accords to Baker et al. (2013) and ULXs with WRL occupy part of XLF in low luminosity region.

For RLOF, their population dominates in XLF and can be divided into two groups according to compact star (BH or NS, see Fig. 1). For less luminous sources, the compact stars of ULXs tend to be BH instead of NS. We note that duration of BH RLOF in high luminosity is significantly longer than NS, and, consequently, more likely to be observed. The mass and radius of NS is lower than BH, and duration of constant mass transfer is harder to maintain before next evolution stage. The typical orbit period for BH via RLOF is a few days and donor star mass tends to be less than 2.7 solar mass. Low initial donor star mass indicates high probability of birth and, correspondingly, larger proportion in population of ULXs. Meanwhile, NS dominates in the region with higher luminosity$L_{app} > 10^{40}erg\cdot s^{-1}$, which is analogous to the previous work (Shao & Li 2015). In our simulation, there is a proven positive correlation between beaming factor and luminosity as shown in Eq. 4. X-ray radiation in BH ULXs is commonly isotropical or mildly-beamed. However, beaming effects is obvious in NS ULXs, and saturated beaming ($b_{min}=3.2\times10^{-3}$see (Lasota et al. 2016)) can be reached in some cases, which is an immediate cause of high luminosity of NS ULXs.

In Fig. 1 (b), we displayed the distribution of Helium rich and Hydrogen rich donor stars. There is evidence showing that evolved donor stars should be the major of ULXs population. For analysis of ULXs' ages, we performed various evolution duration in our simulation, and displayed them in Fig. 2. We ploted the XLF with different color for respective evolution duration. The number of more luminous ULXs significantly drops at an age of 150Myr whose compact star corresponds to NS. When the population is around 30 Myr,

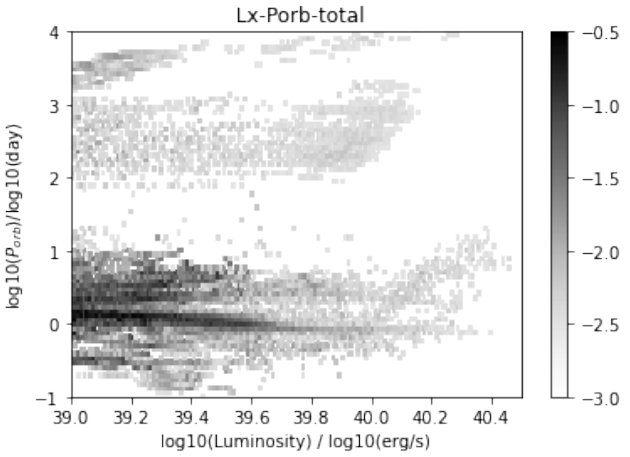

Figure 3. The numerical distribution in the $P_{orb} - L_X$ plane for ULXs. The depth of shade represents the quantity.

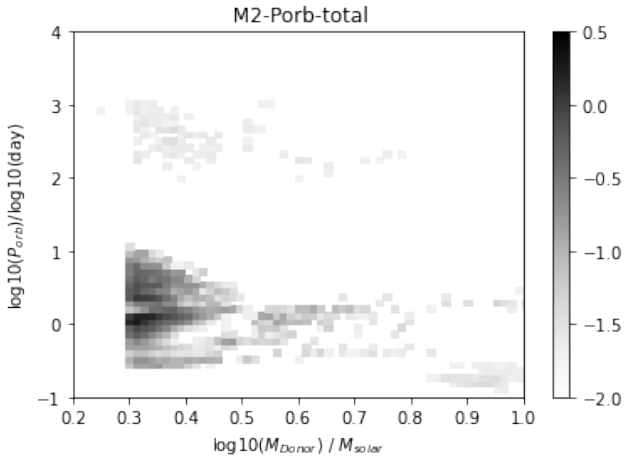

Figure 4. Same as Fig. 3, but for $M_2 - L_X$ plane.

ULXs harboring BH dominate. Galaxies younger than 20 Myr contributes a few because this requires strict condition for rapid formation of compact star. Duration of most young ULXs is usually short so that observation about these binaries is rare. The age of majority of ULXs is around $150Myr$ which indicates that ULXs are the tail evolution stage of HMXBs (Zuo et al. 2014). In our model, population increase after $200Myr$ is not obvious and beyond our consideration in this Ring galaxies case.

Fig. 3 depicts the numerical distribution of ULX with luminosity greater than $10^{39}erg{\cdot}s^{-1}$. The population of each element of this plot is calculated in the same way with XLF. It is seen that binaries with orbit periods shorter than ten days dominate, which corresponds with previous work (Shao & Li 2015). Obviously, the lower luminous region contains more ULXs, same with the differential XLF. Furthermore, detailed analysis indicated that the mass transfer mechanism of ULXs with shorter orbit periods tends to be RLOF while ULXs with WRL are systems with longer orbit period. The donor stars with WRL are more massive in Star-burst galaxies and shorter periods are unstable factor for constant mass transfer. Fig. 4 is the same with Fig. 3 but for $M_2 - L_X$ plane. Due to larger possibility in IMF, lower massive donor star comprise a large proportion. However, ULXs with WRL also contributes to this plot but mass span is large and distribution of each element is tiny. The observation BH ULX cases are rare, and their orbit parameters are difficult to be determined. Liu et al. (2013) has revealed M101 ULX-1 with a BH and a Wolf-Rayet star and confirmed the orbit period being 8.2 days. Later Titarchuk & Seifina (2016) analysed the spectral of M101 and estimated the BH mass on the order of $10^4 M_\odot$ which is an IMBH. We are unable to predict this BH in mass-orbit plane.

4

APPENDIX

4.1 Wind Accretion Efficiency

In the BHL model, the wind accretion efficiency is around 1.5%, which demands high mass transfer rate to form the ULX. The simulation result of wind Roche lobe overflow in HMXB (El Mellah et al. 2019) was adopted, which indicates the relation between accretion efficiency and feature of binaries. Slow acceleration($\beta = 2$) simulation is more realistic for accretion of ULXs due to its high accretion efficiency. In our model, fraction of wind captured is influenced by filling factor and speed ratio for BH and NS respectively. As only typical mass ratio for BH ($q = 2$) and NS ($q = 15$) was obtained via simulation, we assume a linear interpolation for other mass ratio. The typical fraction of wind captured $\mu_{\rm typical}$ is

$$\mu_{\rm typical} = \frac{q_{\rm typical} - q_{\rm NS}}{q_{\rm BH} - q_{\rm NS}}(\mu_{\rm BH} - \mu_{\rm NS}) + \mu_{\rm NS} \qquad (12)$$

where $q_{\rm typical}$ is the particular mass ratio. For other parameters, Nearest neighbor interpolation was performed for more reliable simulation.

4.2 Failure correction

In our statistical model, the summation of star forming probability ought to be equal to 100%. However, a set of particular situations are unrealistic. As a consequence, correction for SFR was implied.

Assuming that all the initial cases are permitted, the integral of probability is

$$\iiint M_1 \epsilon(m_1) \delta \ln M_1 k_q \delta q \dot{k}_a \delta \ln a = 1 \qquad (13)$$

When binaries failed to be generated in failure cases, the integral decrease. In order to normalize the total probability, a correction constant A was multiplied. $A\Sigma Success = A(1 - \Sigma Failure) = 1$

$$A = \frac{1}{1 - \Sigma Failure} \qquad (14)$$

After we performed the simulation and record the probability of Failure cases, A value was obtained via Eq.14. In our model, $A = 1.03$.

ACKNOWLEDGMENTS

This work is supported by the National Natural Science Foundation of China (grant Nos. 11573021, U1938104, 12003020) and the Fundamental Research Funds for the Central Universities.

REFERENCES

Abate C., Pols O. R., Izzard R. G., Mohamed S. S., de Mink S. E., 2013, A&A , 552, A26
Appleton P., Marston A., 1997, The Astronomical Journal, 113, 201
Bachetti M., Harrison F., Walton D. J., Grefenstette B., Chakrabarty D., Fürst F., Barret D., Beloborodov A., Boggs S., Christensen F. E., et al., 2014, Nature, 514, 202
Baker K., MacLaren S., Glendinning G., Seugling R., Whiting N., Source C., Fooks J., Fournier K., Biener M., Martinez D., Smalyuk V., Dittrich T., Moore A., Guymer T., 2013, in APS Division of Plasma Physics Meeting Abstracts Vol. 2013 of APS Meeting Abstracts, Optimizing 9-25 keV point projection 2D backlighters. p. PO7.009
Belczynski K., Kalogera V., Rasio F. A., Taam R. E., Zezas A., Bulik T., Maccarone T. J., Ivanova N., 2008, The Astrophysical Journal Supplement Series, 174, 223
Belczynski K., Ziolkowski J., 2009, The Astrophysical Journal, 707, 870
Blundell K. M., Bowler M. G., Schmidtobreick L., 2007, Astronomy & Astrophysics, 474, 903
Bondi H., Hoyle F., 1944, Monthly Notices of the Royal Astronomical Society, 104, 273
Edgar R., 2004, New Astronomy Reviews, 48, 843
Eggleton P. P., 1983, apj, 268, 368
El Mellah I., Sundqvist J., Keppens R., 2019, Astronomy & Astrophysics, 622, L3
Fürst F., Walton D., Heida M., Harrison F., Barret D., Brightman M., Fabian A., Middleton M., Pinto C., Rana V., et al., 2018, Astronomy & Astrophysics, 616, A186
Gao Y., Wang Q. D., Appleton P., Lucas R. A., 2003, The Astrophysical Journal Letters, 596, L171
Greene J. E., Strader J., Ho L. C., 2020, Annual Review of Astronomy and Astrophysics, 58, 257
Grimm H.-J., Gilfanov M., Sunyaev R., 2003, Monthly Notices of the Royal Astronomical Society, 339, 793
Hobbs G., Lorimer D., Lyne A., Kramer M., 2005, Monthly Notices of the Royal Astronomical Society, 360, 974
Hurley J. R., Tout C. A., Pols O. R., 2002, Monthly Notices of the Royal Astronomical Society, 329, 897
Jiang Y.-F., Stone J. M., Davis S. W., 2014, The Astrophysical Journal, 796, 106
Kaaret P., Feng H., Roberts T. P., 2017, ARAA , 55, 303
King A., 2008, Monthly Notices of the Royal Astronomical Society: Letters, 385, L113
King A., 2009, Monthly Notices of the Royal Astronomical Society: Letters, 393, L41
King A., Lasota J.-P., 2014, Monthly Notices of the Royal Astronomical Society: Letters, 444, L30
King A., Lasota J.-P., 2016, Monthly Notices of the Royal Astronomical Society: Letters, 458, L10
King A., Lasota J.-P., Kluźniak W., 2017, Monthly Notices of the Royal Astronomical Society: Letters, 468, L59
King A. R., Davies M. B., Ward M. J., Fabbiano G., Elvis M., 2001, The Astrophysical Journal, 552, L109
Kovlakas K., Zezas A., Andrews J. J., Basu-Zych A., Fragos T., Hornschemeier A., Lehmer B., Ptak A., 2020
Kroupa P., Tout C. A., Gilmore G., 1993, Monthly Notices of the Royal Astronomical Society, 262, 545
Kuranov A., Popov S., Postnov K., Volonteri M., Perna R., 2007, Monthly Notices of the Royal Astronomical Society, 377, 835
Lamers H. J., Snow T. P., Lindholm D. M., 1995, The Astrophysical Journal, 455, 269
Lasota J.-P., Vieira R., Sadowski A., Narayan R., Abramowicz M., 2016, Astronomy & Astrophysics, 587, A13
Liu J.-F., Bregman J. N., Bai Y., Justham S., Crowther P., 2013, Nature, 503, 500
Middleton M., Brightman M., Pintore F., Bachetti M., Fabian A., Fuerst F., Walton D., 2019, Monthly Notices of the Royal Astronomical Society, 486, 2
Middleton M. J., King A., 2017, Monthly Notices of the Royal Astronomical Society: Letters, 470, L69
Mineo S., Gilfanov M., Sunyaev R., 2012, Monthly Notices of the Royal Astronomical Society, 419, 2095
Mineo S., Rappaport S., Steinhorn B., Levine A., Gilfanov M., Pooley D., 2013, Astrophysical Journal, 771
Mohamed S., Podsiadlowski P., 2011, in Kerschbaum F., Lebzelter T., Wing R. F., eds, Why Galaxies Care about AGB Stars II: Shining Examples and Common Inhabitants Vol. 445 of Astronomical Society of the Pacific Conference Series, Wind Roche-Lobe Overflow: A New Mass Transfer Mode for Mira-type Binaries. p. 355
Ohsuga K., Mineshige S., 2011, The Astrophysical Journal, 736, 2
Poutanen J., Lipunova G., Fabrika S., Butkevich A. G., Abolmasov P., 2007, Monthly Notices of the Royal Astronomical Society, 377, 1187
Shakura N. I., Sunyaev R. A., 1973, Astronomy and Astrophysics, 24, 337
Shao Y., Li X. D., 2015, Astrophysical Journal, 802
Shao Y., Li X.-D., Dai Z.-G., 2019, ApJ , 886, 118
Swartz D. A., Soria R., Tennant A. F., Yukita M., 2011, Astrophysical Journal, 741
Titarchuk L., Seifina E., 2016, Astronomy & Astrophysics, 585, A94
Wang S., Qiu Y., Liu J., Bregman J. N., 2016, The Astrophysical Journal, 829, 20
Webbink R., 1984, The Astrophysical Journal, 277, 355
Webbink R. F., 2008, in , Short-Period Binary Stars: Observations, Analyses, and Results. Springer, pp 233–257
Wiktorowicz G., Lasota J.-P., Middleton M., Belczynski K., 2019a, The Astrophysical Journal, 875, 53
Wiktorowicz G., Lasota J.-P., Middleton M., Belczynski K., 2019b, The Astrophysical Journal, 875, 53
Wiktorowicz G., Sobolewska M., Lasota J.-P., Belczynski K., 2017, The Astrophysical Journal, 846, 17
Wolter A., Consolandi G., Longhetti M., Landoni M., Bianco A., 2018, Proceedings of the International Astronomical Union, 14, 297–306
Wolter A., Esposito P., Mapelli M., Pizzolato F., Ripamonti E., 2015, Monthly Notices of the Royal Astronomical Society, 448, 781
Wolter A., Fruscione A., Mapelli M., 2018a, The Astro-

physical Journal, 863, 43
Wolter A., Fruscione A., Mapelli M., 2018b, The Astrophysical Journal, 863, 43
Yungelson L., Livio M., Tutukov A., 1997, The Astrophysical Journal, 481, 127
Zuo Z.-Y., Li X.-D., 2014, Monthly Notices of the Royal Astronomical Society, 442, 1980
Zuo Z.-Y., Li X.-D., Gu Q.-S., 2014, Monthly Notices of the Royal Astronomical Society, 437, 1187
Zuo, Zhao-Yu Song, Hao-Tian Xue, Han-Chen 2021, A&A, 649, L2